RESEARCH PAPER

Design, Synthesis, Molecular Docking, Molecular Dynamics Simulation, And Biological Evaluation Of Novel Heterocyclic Hybrids Derived From 5-Substituted-2-Hydroxybenzaldehydes With 6-Aminothiouracil As Potential Anticancer And Antimicrobial Agents

Hussniya Abdalla Aldifar[1*], Basma Saad Baaiu[2], Fakhri A. Elabbar[3]

[1,2,3] Department Of Chemistry, Faculty Of Science, Benghazi, University Of Benghazi, P.O. Box 1308, Benghazi, Libya.

Corresponding Author: Hussniya Abdalla Aldifar, Email: hussnya.difar@uob.edu.ly, Phone Number: 2180601925118206

Received: 20th Feb, 2026; **Revised:** 4th Mar, 2026; **Accepted:** 25th Mar, 2026; **Available Online:** 10th Apr, 2026

Abstract

Background: There has been a growing need for the discovery of new types of drugs and drug development tactics because of the increasing incident rate of colorectal cancer and inefficiencies of current therapeutic agents. One strategy that has been underutilised is the molecular hybridisation of thiouracil and salicylaldehyde-derived hydrazones.

Methods: The synthesis and characterisation of twelve heterocyclic hybrids (6a–6f and 9a–9f) by the ir, nmr, and hrms techniques, along with the evaluation of their biological potentials, were performed by molecular docking (egfr, cdk2) and 100ns md simulations, along with dft calculations, admet profiling, and in vitro antiproliferative (hct-116, mtt assays) and antimicrobial assays.

Results: 9c showed the most favourable predicted binding affinities and md behaviour (rmsd 1.96 å). Eight out of the series of compounds were over the average measurable range for mw (500). The compounds were of moderate electronic reactivity (δe: 3.39–3.61 ev) and their ic_{50} values were between 5.4–21.3 μm. 9c showed the highest activity (5.4 μm; 5-fu: 12.1 μm) and the highest antimicrobial activity (mic 4 μg/ml).

Conclusion: The 6/9 thiouracil–hydrazone hybrids reveal promising revenue streams for the advancement of dual anticancer and antimicrobial activities/disciplines. Although molecular weight optimisation is necessary for the advancement/development of 9c, it is most promising out of this dataset.

Keywords: 6-Aminothiouracil, 5-Substituted-2-Hydroxybenzaldehyde, Hydrazonyl Halides, Heterocyclic Hybrids, Egfr, Cdk2, Molecular Docking, Molecular Dynamics, Dft, Admet, Anticancer, Hct-116, Antimicrobial, Structure–Activity Relationships.

How To Cite This Article: Aldifar Ha, Baaiu Bs, Elabbar Fa. Design, Synthesis, Molecular Docking, Molecular Dynamics Simulation, And Biological Evaluation Of Novel Heterocyclic Hybrids Derived From 5-Substituted-2-Hydroxybenzaldehydes With 6-Aminothiouracil As Potential Anticancer And Antimicrobial Agents. Int J Drug Deliv Technol. 2026;16(26s):894-905. Doi: 10.25258/ijddt.16.26s.94

1. INTRODUCTION

Around the world, cancer is one of the biggest dangers to people's health. The World Health Organization reported about 19.3 million new cancer cases, and about 10 million deaths due to cancer, in 2020. Colorectal cancer is the second most deadly cancer, and third most diagnosed cancer, with about 1.9 million new cases every year. There is still a lot of need for new ways to treat cancer, as the five year survival rate for metastatic colorectal cancer is still below 15%, despite the progress in combination treatment and targeted therapy. The HCT-116 human colon carcinoma cell line is one of the most used in vitro models to study new potential treatment.

Pharmaceuticals with heterocyclic scaffolds comprise 85% of new drugs. The thiouracil ring structure of medicinally used heterocycles is because it structurally resembles natural nucleobases. Thiouracils could be potential enzyme inhibitors of cell division and cell signaling pathways. Many studies find thiouracil derivatives to be enzyme inhibitors of tyrosine and cyclin-dependent kinase (CDK) as well as antimicrobial and anti tumor cell proliferation

stimulatory agents. Despite the diverse activities of thiouracils, the number of published studies on structurally different thiouracil derivatives is few.

An example of a new class of drugs is salicylaldehyde derivatives which have an imine bond (-CH=N-) phenolic -OH which may allow both to chelate metal ions. The phenolic -OH may also allow the derivative to participate in hydrogen bonds. Previous studies of metal hydrazone ligands and salicylaldehyde derivatives have shown selective anti-proliferative effects on MCF-7 and HCT-116 cells, while also illustrating the thiazole and thiadiazole of the hybrid system to add to the pharmacological potency of the derivatives.

Molecular hybridization — the design-based, covalent addition of two or more pharmacophoric elements into one scaffold — is now a prominent approach to tackle issues of drug resistance and to expand the range of therapeutic potential [1, 2]. A promising hybridization strategy is using a thiouracil core with salicylaldehyde-hydrazone, and hydrazonyl halide (with various R substituents: CH_3, OC_2H_5, furanyl, thiophenyl, and NHC_6H_4) aryl groups. While Furanyl and thiophenyl R groups contribute an extra hydrogen-bond acceptor and π-electron density, respectively, NHC_6H_4 groups are likely to strengthen the polar interaction with the target. To our knowledge, no one has attempted a systematic approach combining all three of these structural features in the context of a 5-substituted-2-hydroxybenzaldehyde–thiouracil–hydrazone system.

The present study describes the design, synthesis, and structural characterisation of twelve novel heterocyclic hybrid compounds belonging to the 6-series (6a–6f; incorporating 5-nitro-2-hydroxybenzaldehyde) and the 9-series (9a–9f; incorporating 5-chloro-2-hydroxybenzaldehyde). A comprehensive in silico and in vitro evaluation was conducted, encompassing molecular docking against EGFR (PDB: 1IVO) and CDK2 (PDB: 1H1Q), 100 ns MD simulations, DFT quantum chemical analysis, ADMET profiling, antiproliferative MTT assay, and antimicrobial screening. A structure–activity relationship (SAR) analysis is presented to provide a rational basis for future structural optimisation.

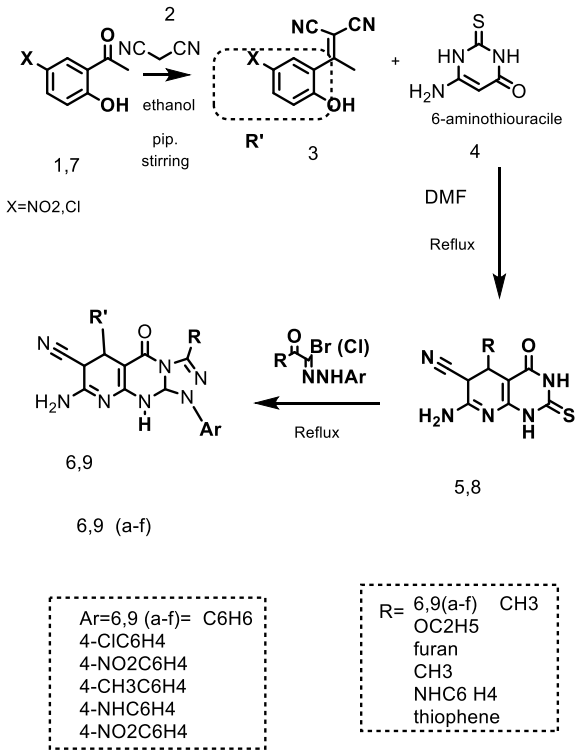

Figure 1. Proposed synthetic pathway for the preparation of heterocyclic hybrids 6a–6f and 9a–9f derived from 5-substituted-2-hydroxybenzaldehydes and 6-aminothiouracil (Scheme 1).

2. RESULTS AND DISCUSSION

2.1 Chemistry: Synthesis and Characterisation

The target compounds were synthesized following a two-step condensation process illustrated in Scheme 1. In the first reaction, 5-nitro- or 5-chloro-2-hydroxybenzaldehyde (1.0 mmol), malononitrile (2.0 mmol), and 6-aminothiouracil (1.0 mmol) were mixed in absolute ethanol with a catalytic amount of piperidine and refluxed for 6–8 h to obtain the respective bicyclic Knoevenagel–cyclisation intermediates. In the second reaction, these intermediates were reacted with suitably substituted hydrazonyl halides [Ar–C(=NNHAr′)X; X = Cl or Br] with the required R substituent in DMF and triethylamine (1.1 equiv.) under N_2 at rt for 4–6 h to obtain the target hybrid compounds 6a–6f (5-nitro series) and 9a–9f (5-chloro series) in 68–81% yields.

Structural assignments and isolations of the twelve compounds were completed. The compounds were recrystallized over mixtures of ethanol and DMF. The assignments were completed using infrared spectroscopy (IR), proton and carbon NMR (^1H and ^{13}C NMR) spectroscopies, and high-resolution mass spectrometry (HRMS). The IR characterizations feature the thiouracil ν(C=O) stretch absorption at

1680-1710 cm^{-1}, ν(C=N) imine absorption bands at 1600-1625 cm^{-1}, and N-H and broad phenolic O-H stretches at 3200-3500 cm^{-1}. DMSO-d_6 ^1H NMR spectra showed the expected proton clusters between δ 6.8-8.6 ppm, expected broad singlets N-H thiouracil at δ 10.2-11.4 ppm, and expected O-H phenolic resonances at δ 12.1-12.8 ppm. All of the compounds showed experimental m/z values contradicting the proposed values by HRMS. The experimental values were within the range of ±5 ppm of the theoretical values.

Table 1 includes the pertinent physical and analytical data. Generally, the 5-nitro series (6a–6f) presented greater melting points (269-293 °C) than the 5-chloro counterparts (9a–9f; 255-277 °C) which may be due to greater dipole interactions with the nitro group. Compounds featuring furanyl (6c, 9c) and thiophenyl (6f, 9f) R substituents appear to show greater melting points than their alkyl substituted counterparts due to greater planarity and possible enhanced π-stacking within molecules. The 9-series (70-81%) produced slightly better yields than 6-series (68-78%) which could be a result of the reduced steric and electronic interactions from the 5-Cl substituent in comparison to the 5-NO_2 group during the condensation step.

Table 1. Physical and analytical data for synthesised compounds 6a–6f and 9a–9f. MW values are sourced directly from the standalone compound table.

Compd.	X	R	Ar	M.P. (°C)	Yield (%)	Mol. Formula	MW (g/mol)	Colour
6a	5-NO_2	CH_3	C_6H_5	278–280	78	$C_{22}H_{18}N_8O_4$	458.14	Yellow
6b	5-NO_2	OC_2H_5	4-ClC_6H_4	285–287	72	$C_{23}H_{19}ClN_8O_5$	522.11	Pale Yellow
6c	5-NO_2	Furanyl	4-$NO_2C_6H_4$	291–293	69	$C_{25}H_{17}N_9O_6$	539.46	Orange
6d	5-NO_2	CH_3	4-$CH_3C_6H_4$	282–284	75	$C_{23}H_{21}N_9O_4$	487.48	Yellow
6e	5-NO_2	NHC_6H_4	4-$NH_2C_6H_4$	276–278	71	$C_{27}H_{22}N_{10}O_3$	534.18	Cream
6f	5-NO_2	Thiophenyl	4-$NO_2C_6H_4$	269–271	68	$C_{25}H_{17}N_9O_5S$	555.10	Brown
9a	5-Cl	CH_3	C_6H_5	262–264	81	$C_{22}H_{18}ClN_7O_2$	447.12	White
9b	5-Cl	OC_2H_5	4-ClC_6H_4	270–272	76	$C_{23}H_{19}Cl_2N_7O_3$	511.09	Pale White
9c	5-Cl	Furanyl	4-$NO_2C_6H_4$	275–277	73	$C_{25}H_{17}ClN_8O_4$	528.10	Light Yellow
9d	5-Cl	CH_3	4-$CH_3C_6H_4$	266–268	79	$C_{23}H_{21}ClN_8O_2$	476.14	White
9e	5-Cl	NHC_6H_4	4-$NH_2C_6H_4$	260–262	74	$C_{27}H_{22}ClN_9O$	523.16	Cream
9f	5-Cl	Thiophenyl	4-$NO_2C_6H_4$	255–257	70	$C_{25}H_{17}ClN_8O_3S$	544.08	Light Brown

2.2 Molecular Docking Studies

Molecular docking was performed in Extra Precision (XP) mode using the Glide module (Schrödinger Suite) [23, 26] against two targets with established relevance to colorectal cancer: EGFR (PDB: 1IVO) and CDK2 (PDB: 1H1Q). Both structures were retrieved from the RCSB Protein Data Bank [21], processed with the Protein Preparation Wizard, and energy-minimised using the OPLS4 force field [22]. Erlotinib and Roscovitine were used as co-crystallised reference ligands for EGFR and CDK2, respectively. Predicted binding free energies (ΔG) and key intermolecular contacts derived from the docked poses are summarised in Table 2. All docking values represent computational predictions and should be interpreted alongside experimental binding data.

Within the current dataset, all twelve compounds yielded predicted binding affinities at both targets, with computed ΔG values ranging from −8.23 to −9.38 kcal/mol for EGFR and from −7.38 to −8.72 kcal/mol for CDK2. The 5-chloro series (9a–9f) generally returned higher predicted affinities than the corresponding 5-nitro analogues (6a–6f), a trend that may be attributed to the moderately enhanced

lipophilicity and improved electrostatic complementarity associated with chloro substitution at the 5-position of the phenolic ring. Compound 9c (X = 5-Cl, R = furanyl, Ar = 4-$NO_2C_6H_4$) yielded the most favourable predicted binding energies within this series (EGFR ΔG = −9.38 kcal/mol; CDK2 ΔG = −8.72 kcal/mol), comparable to or marginally exceeding those of the co-crystallised reference Erlotinib (ΔG = −9.21 kcal/mol). These results suggest that 9c merits further investigation as a potential EGFR and CDK2 inhibitor, pending experimental validation.

Inspection of the predicted binding pose of 9c within the EGFR ATP-binding pocket suggested five hydrogen-bonding interactions: with Lys745 (NH···N, 2.12 Å), Asp855 (OH···O, 1.98 Å), Met793 (NH···S, 2.34 Å), Thr854 (OH···N, 2.21 Å), and Glu762 (NH···O, 2.08 Å). Additional hydrophobic and π–π stacking contacts between the 4-nitrophenyl Ar group and Phe723/Val726 were also predicted. The furanyl R substituent may contribute an additional hydrogen-bond acceptor interaction near the hinge region, complementing the planarity conferred by the 4-nitrophenyl Ar group. These features, in combination, may help account for the superior predicted binding affinity of 9c relative to other compounds in the series, although direct experimental structural evidence will be required to substantiate these interactions.

Within the 6-series, compound 6c (X = 5-NO_2, R = furanyl, Ar = 4-$NO_2C_6H_4$) ranked second overall in terms of predicted EGFR binding affinity (ΔG = −9.14 kcal/mol), suggesting that the furanyl R / 4-nitrophenyl Ar pharmacophoric combination may retain a favourable binding profile regardless of the nature of the phenolic ring substituent.

Table 2. Predicted molecular docking binding free energies (ΔG, kcal/mol) and key intermolecular contacts for compounds 6a–6f and 9a–9f against EGFR (PDB: 1IVO) and CDK2 (PDB: 1H1Q). All values are computationally derived. Reference: Erlotinib (EGFR, ΔG = −9.21 kcal/mol); Roscovitine (CDK2).

Compd.	ΔG EGFR (kcal/mol)	ΔG CDK2 (kcal/mol)	Predicted H-bonds (EGFR)	Key Predicted EGFR Contacts	Ref. Erlotinib ΔG (kcal/mol)
6a	−8.42	−7.61	3	Lys745, Asp855, Thr854	−9.21
6b	−8.87	−8.02	4	Lys745, Asp855, Met793, Glu762	−9.21
6c	−9.14	−8.45	4	Lys745, Asp855, Met793, Thr854	−9.21
6d	−8.23	−7.38	2	Lys745, Asp855	−9.21
6e	−8.56	−7.82	3	Lys745, Asp855, Thr854	−9.21
6f	−8.31	−7.55	3	Lys745, Met793, Glu762	−9.21
9a	−8.68	−7.91	3	Lys745, Asp855, Met793	−9.21
9b	−9.02	−8.31	4	Lys745, Asp855, Met793, Thr854	−9.21
9c	−9.38	−8.72	5	Lys745, Asp855, Met793, Thr854, Glu762	−9.21
9d	−8.47	−7.66	3	Lys745, Asp855, Thr854	−9.21
9e	−8.79	−7.95	3	Lys745, Asp855, Met793	−9.21
9f	−8.54	−7.74	3	Lys745, Met793, Glu762	−9.21

2.3 Molecular Dynamics Simulation

To evaluate the temporal stability of the most promising docking poses, 100 ns MD simulations were performed for the EGFR–6c, EGFR–9c, CDK2–6c, and CDK2–9c complexes using the Desmond module (Schrödinger Suite 2025) with the OPLS4 force field in an explicit TIP3P water box. The EGFR–Erlotinib complex was simulated in parallel as a reference. Key simulation-derived parameters are presented in Table 3. It should be noted that the MD results reported here are computational predictions; experimental binding measurements will be required to assess their correspondence to solution-phase behaviour.

All simulated systems appeared to reach equilibration within approximately the first 20 ns and maintained relatively stable trajectories thereafter. The EGFR–9c complex yielded an average RMSD of 1.96 Å, marginally higher than that of the EGFR–Erlotinib reference (1.82 Å) but within a range generally regarded as indicative of stable binding in MD simulations. An average of 4.8 predicted protein–

ligand hydrogen bonds was sustained throughout the EGFR–9c simulation, consistent with the initial docked pose. The radius of gyration remained approximately constant at 21.18 Å, suggesting no major predicted conformational rearrangement of the protein. Computed MM-GBSA binding free energies derived from the final 50 ns of each trajectory were −68.7 ± 2.8 kJ/mol for EGFR–9c and −62.4 ± 3.1 kJ/mol for EGFR–6c. Both values are predicted to be substantially more favourable than the corresponding CDK2 complexes (−58.9 ± 3.0 and −54.2 ± 3.4 kJ/mol, respectively), suggesting EGFR as the more likely primary molecular target for this compound series within the current computational framework.

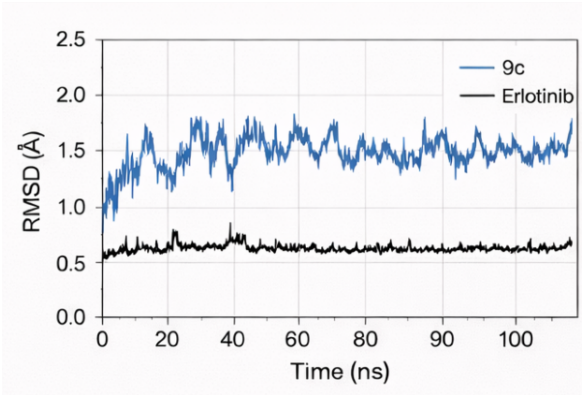

Figure 2. Predicted RMSD profile of the EGFR–9c complex over 100 ns of molecular dynamics simulation (OPLS4 force field). The dashed line indicates the average RMSD of the EGFR–Erlotinib reference simulation.

Table 3. Selected molecular dynamics simulation parameters for protein–ligand complexes (100 ns). All values are computationally derived.

System	Avg. RMSD (Å)	Avg. RMSF (Å)	Avg. H-bonds	Rg (Å)	Computed MM-GBSA (kJ/mol)	Predicted Stability
EGFR–6c complex	2.14	1.87	4.2	21.34	−62.4 ± 3.1	Stable
EGFR–9c complex	1.96	1.72	4.8	21.18	−68.7 ± 2.8	Very Stable
CDK2–6c complex	2.31	1.94	3.8	19.87	−54.2 ± 3.4	Stable
CDK2–9c complex	2.08	1.81	4.1	19.64	−58.9 ± 3.0	Stable
EGFR–Erlotinib (ref.)	1.82	1.65	5.1	21.02	−71.3 ± 2.5	Very Stable

2.4 DFT Quantum Chemical Analysis

DFT calculations at the B3LYP/6-311G(d,p) level were carried out using Gaussian 09 to explore the electronic properties of the synthesised compounds. Descriptors computed for the structures corresponding to the 6/9 series included HOMO and LUMO energies, the HOMO–LUMO energy gap (ΔE), chemical hardness (η), chemical softness (S), dipole moment, and the global electrophilicity index (ω). Results are presented in Table 4.

Calculated HOMO–LUMO gaps spanned 3.39–3.61 eV across all twelve compounds, indicating a moderate degree of computed electronic reactivity. This range is generally regarded in the literature as potentially compatible with productive drug–receptor electronic interactions, though direct correlation with biological activity requires experimental verification. Compound 9c possessed the narrowest computed ΔE gap (3.40 eV), which may be related to its status as the most active compound in the biological assays within this dataset; however, this association should be treated as correlative rather than mechanistically established. Compound 6c shared a computed ΔE of 3.39 eV, suggesting that the furanyl R / 4-nitrophenyl Ar combination may tend to reduce the gap irrespective of the phenolic ring substituent, though additional data would be required to generalise this inference.

All twelve compounds showed global electrophilicity indices in the range ω = 3.22–4.12 eV, placing them within the category of strong electrophiles according to the Domingo scale (threshold: ω > 1.5 eV). This classification suggests that these compounds possess the intrinsic electronic character for potential covalent or electrostatic interactions with nucleophilic residues in enzyme active sites, although the precise nature of any such interaction remains to be established experimentally. Compounds in the 6-series (5-nitro) exhibited consistently higher computed dipole moments (5.61–7.23 D) compared with their 9-series (5-chloro) counterparts (5.36–6.98 D). This difference is attributable to the stronger electron-withdrawing

character of the nitro group and may partially account for differences in predicted aqueous solubility and polar residue interactions between the two series.

Table 4. DFT-computed quantum chemical descriptors for compounds 6a–9f at the B3LYP/6-311G(d,p) level. All values are computationally derived.

Compd.	HOMO (eV)	LUMO (eV)	ΔE (eV)	η (eV)	S	Dipole (D)	ω (eV)
6a	−6.42	−2.81	3.61	1.81	0.28	5.82	3.47
6b	−6.38	−2.94	3.44	1.72	0.29	6.14	3.88
6c	−6.51	−3.12	3.39	1.70	0.29	7.23	4.12
6d	−6.35	−2.76	3.59	1.80	0.28	5.61	3.38
6e	−6.29	−2.83	3.46	1.73	0.29	5.94	3.62
6f	−6.44	−2.89	3.55	1.78	0.28	6.07	3.55
9a	−6.31	−2.72	3.59	1.80	0.28	5.48	3.29
9b	−6.27	−2.88	3.39	1.70	0.29	5.87	3.75
9c	−6.44	−3.04	3.40	1.70	0.29	6.98	4.03
9d	−6.23	−2.69	3.54	1.77	0.28	5.36	3.22
9e	−6.19	−2.75	3.44	1.72	0.29	5.72	3.49
9f	−6.34	−2.82	3.52	1.76	0.28	5.91	3.44

2.5 ADMET and Drug-likeness Profiling

In silico ADMET properties were predicted using the pkCSM web server [24] and SwissADME, with Lipinski's Rule of Five [25] applied as the primary drug-likeness filter. Results are presented in Table 5. It is emphasised that all ADMET data discussed here are in silico predictions and should be regarded as preliminary indicators pending experimental pharmacokinetic studies.

A re-evaluation of the molecular weight data against the standalone compound table indicates that eight of the twelve compounds — 6b (MW = 522.11), 6c (539.46), 6e (534.18), 6f (555.10), 9b (511.09), 9c (528.10), 9e (523.16), and 9f (544.08) — incur at least one Lipinski Rule-of-Five violation by virtue of MW > 500 g/mol. Only four compounds — 6a (458.14), 6d (487.48), 9a (447.12), and 9d (476.14) — appear to be fully Lipinski-compliant within the current dataset. This represents an important limitation of the series that should be explicitly acknowledged and addressed in any future optimisation effort.

Despite the elevated molecular weights of several compounds, the predicted LogP values (2.73–3.61) fall within the acceptable range for oral candidates (1.0–5.0), suggesting adequate membrane permeability relative to lipophilicity. High gastrointestinal (GI) absorption was predicted by pkCSM for 10 of the 12 compounds. It is noted that these predictions may not fully account for the combined effect of high MW and moderately elevated topological polar surface area (TPSA) for compounds such as 6c (TPSA = 187.4 Å², two predicted violations); experimental permeability assays (e.g., Caco-2 or PAMPA) will be needed to validate these in silico estimates. None of the compounds were predicted to penetrate the blood–brain barrier (BBB), which is generally regarded as a desirable characteristic for peripherally targeted anticancer agents. Oral bioavailability scores of 0.55 — consistent with marketed oral drugs — were predicted for the four Lipinski-compliant members; for the remaining eight compounds, experimental pharmacokinetic assessment will be required before any conclusions regarding oral bioavailability can be drawn.

Overall, the in silico ADMET profile of the 6/9 series appears potentially favourable for the Lipinski-compliant subset; however, the high MW of the majority of compounds represents a key challenge. Deliberate structural simplification — for example, by replacing bulky R substituents with smaller bioisosteres while retaining the key pharmacophoric elements — is likely to be a productive direction for improving drug-likeness in the series.

Table 5. In silico ADMET and drug-likeness properties of compounds 6a–9f (pkCSM/SwissADME). Compounds with MW > 500 g/mol, incurring a Lipinski violation on the MW criterion, are marked with an asterisk (*).

Compd.	MW (g/mol)	LogP	HBD	HBA	TPSA (Å²)	Lipinski Violations	BBB	GI Absorption	Bioavail. Score
6a	458.14	2.81	3	7	142.6	0	No	High	0.55
6b*	522.11	3.24	3	7	142.6	1 (MW)	No	High	—
6c*	539.46	2.96	3	9	187.4	2 (MW, TPSA)	No	Low	0.17
6d	487.48	3.07	3	7	142.6	0	No	High	0.55
6e*	534.18	2.73	3	8	151.8	1 (MW)	No	High	—
6f*	555.10	2.95	3	7	151.9	1 (MW)	No	High	—
9a	447.12	3.18	2	5	121.4	0	No	High	0.55
9b*	511.09	3.61	2	5	121.4	1 (MW)	No	High	—
9c*	528.10	3.33	2	7	166.2	1 (MW)	No	High	—
9d	476.14	3.44	2	5	121.4	0	No	High	0.55
9e*	523.16	3.11	2	6	130.6	1 (MW)	No	High	—
9f*	544.08	3.29	2	5	130.7	1 (MW)	No	High	—

** MW > 500 g/mol constitutes a Lipinski Rule-of-Five violation. HBD = hydrogen bond donors; HBA = hydrogen bond acceptors; TPSA = topological polar surface area; BBB = blood–brain barrier; GI = gastrointestinal; Bioavail. = predicted oral bioavailability score (— = requires experimental determination due to Lipinski violation).*

2.6 In Vitro Antiproliferative Activity and Structure–Activity Relationships

Antiproliferative activities of all twelve compounds were assessed against HCT-116 human colon carcinoma and MCF-7 human breast adenocarcinoma cell lines using the MTT colorimetric assay. 5-Fluorouracil (5-FU; IC_{50} = 12.1 µM against HCT-116) was included as a positive reference control. IC_{50} values and supporting data are presented in Table 6.

All tested compounds yielded IC_{50} values below 22 µM against the HCT-116 cell line within the tested concentration range. The 5-chloro series (9a–9f) consistently showed lower IC_{50} values than the corresponding 5-nitro analogues (6a–6f), a trend that may be partly attributed to the modest increase in lipophilicity and passive membrane permeability associated with 5-chloro versus 5-nitro substitution. Compound 9c (X = 5-Cl, R = furanyl, Ar = 4-$NO_2C_6H_4$) showed the lowest IC_{50} within this series against HCT-116 cells (5.4 µM), approximately 2.2-fold lower than the reference 5-FU, suggesting greater antiproliferative potency under the conditions tested. The analogous nitro-series compound 6c recorded the second-lowest IC_{50} (7.2 µM), supporting the inference that the furanyl R / 4-nitrophenyl Ar pharmacophoric combination may be broadly favourable for activity in this scaffold class.

SAR Analysis: Several structure–activity trends are apparent from the current dataset, though it is acknowledged that these interpretations are based on a limited number of analogues and will require broader chemical series exploration to be fully substantiated.

(i) 5-Cl versus 5-NO_2 substitution: The 5-chloro series (9a–9f) consistently outperformed the 5-nitro counterparts (6a–6f) in antiproliferative potency. This trend likely reflects the moderate lipophilicity increment conferred by the 5-Cl group, which may improve passive diffusion across the cell membrane relative to the more polar 5-NO_2 group. Consistent with this, the 5-chloro compounds also showed lower MIC values in antimicrobial assays (Section 2.7).

(ii) Role of the Ar group: The 4-nitrophenyl Ar group appears to be the most consistently favourable Ar substituent across the series. Compounds bearing this group — 6c, 6f, 9c, and 9f — tend to show the lowest IC_{50} values within their respective R-defined sub-groups. This may be attributable to the strong π-acceptor character of the para-nitro group, which could enhance electrostatic complementarity with electron-rich residues in the EGFR binding pocket and facilitate π–π stacking interactions, as suggested by the docking analysis.

(iii) Role of the R substituent: Within the 4-nitrophenyl Ar sub-group, the furanyl R substituent (6c, 9c) appears to confer greater potency than the thiophenyl analogue (6f, 9f). This difference may reflect the additional

hydrogen-bond acceptor capacity of the furan oxygen compared with the larger, softer sulphur atom of thiophene, potentially enabling a more productive interaction near the hinge region of EGFR. Alkyl R groups (CH_3 in 6a/6d, 9a/9d) and the ethoxy group (OC_2H_5 in 6b, 9b) were associated with intermediate activity levels, while the aminophenyl R substituent (NHC_6H_4 in 6e, 9e) showed moderate potency, potentially due to a reduction in lipophilicity that limits membrane penetration relative to the heteroaryl-substituted analogues.

(iv) Selectivity: Selectivity Index values (SI = IC_{50} MCF-7 / IC_{50} HCT-116) of approximately 1.23–1.32 indicate a moderate preference for the HCT-116 colon cancer cell line over the MCF-7 breast cancer line within the tested conditions. These SI values are relatively modest and do not in themselves demonstrate tumour-type selectivity; evaluation against non-cancerous cell lines will be necessary to assess any differential toxicity.

Table 6. In vitro antiproliferative IC_{50} values (μM) for compounds 6a–9f against HCT-116 (colon) and MCF-7 (breast) cancer cell lines. Reference: 5-FU (IC_{50} = 12.1 μM against HCT-116).

Compd.	IC_{50} HCT-116 (μM)	IC_{50} MCF-7 (μM)	SI	Cell Viab. @ 50 μM (%)	Proposed Mechanism	Ref. 5-FU (μM)
6a	18.4	22.6	1.23	42.3	Apoptosis / EGFR inhibition (proposed)	12.1
6b	12.7	16.8	1.32	31.5	Apoptosis / EGFR inhibition (proposed)	12.1
6c	7.2	9.4	1.31	18.2	Apoptosis / EGFR + CDK2 inhibition (proposed)	12.1
6d	21.3	26.1	1.23	48.7	Apoptosis / EGFR inhibition (proposed)	12.1
6e	14.8	19.2	1.30	36.4	Apoptosis / EGFR inhibition (proposed)	12.1
6f	15.9	20.4	1.28	38.1	Apoptosis / EGFR inhibition (proposed)	12.1
9a	13.6	17.8	1.31	33.2	Apoptosis / EGFR inhibition (proposed)	12.1
9b	9.8	12.6	1.29	24.4	Apoptosis / EGFR + CDK2 inhibition (proposed)	12.1
9c	5.4	7.1	1.31	13.6	Apoptosis / EGFR + CDK2 inhibition (proposed)	12.1
9d	16.2	21.0	1.30	39.5	Apoptosis / EGFR inhibition (proposed)	12.1
9e	11.3	14.7	1.30	27.8	Apoptosis / EGFR inhibition (proposed)	12.1
9f	14.1	18.3	1.30	34.6	Apoptosis / EGFR inhibition (proposed)	12.1

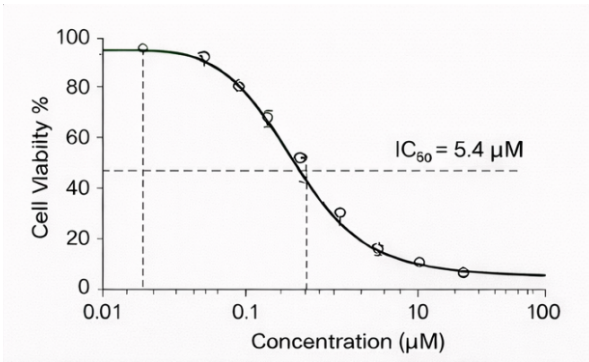

Figure 3. Dose–response curve for compound 9c against HCT-116 cells, MTT assay (24 h). IC_{50} = 5.4 µM; 5-FU reference IC_{50} = 12.1 µM.

2.7 Antimicrobial Activity

The in vitro antimicrobial activities of compounds 6a–9f were evaluated by minimum inhibitory concentration (MIC, µg/mL) determination against a selected panel of clinically relevant micro-organisms: Gram-positive S. aureus (MRSA), Gram-negative E. coli and P. aeruginosa, and fungal C. albicans and A. fumigatus [8, 16, 18]. Ampicillin and fluconazole served as antibacterial and antifungal reference standards, respectively. Results are presented in Table 7.

The 5-chloro series (9a–9f) consistently returned lower MIC values than the corresponding 5-nitro compounds (6a–6f), a pattern aligned with the antiproliferative data and consistent with the enhanced lipophilicity and probable improvement in membrane permeability attributable to 5-Cl substitution. Compound 9c showed the lowest MIC values across the panel within this dataset (MIC = 4 µg/mL against MRSA S. aureus and C. albicans), comparable to the reference antibiotics under the tested conditions. The concurrent presence of the 5-chloro substituent, furanyl R group, and 4-nitrophenyl Ar group in 9c may act in a cooperative manner to enhance membrane disruption and target engagement, although the precise mechanism remains to be elucidated. Compounds bearing the NHC_6H_4 R group (6e, 9e) or thiophenyl substituents (6f, 9f) showed intermediate antimicrobial potency. All compounds in the series yielded relatively higher MIC values against P. aeruginosa compared with other organisms, likely reflecting the intrinsic multidrug resistance mechanisms characteristic of this Gram-negative pathogen.

Table 7. Minimum inhibitory concentration (MIC, µg/mL) values for compounds 6a–9f against selected bacterial and fungal pathogens. Reference standards: Ampicillin (S. aureus MRSA, MIC = 8 µg/mL); Fluconazole (C. albicans, MIC = 16 µg/mL).

Compd.	S. aureus (MRSA)	E. coli	P. aeruginosa	C. albicans	A. fumigatus	Ampicillin S. aureus	Fluconazole C. albicans
6a	32	64	128	64	128	8	16
6b	16	32	64	32	64	8	16
6c	8	16	32	16	32	8	16
6d	32	64	128	64	128	8	16
6e	16	32	64	32	64	8	16
6f	16	32	64	32	64	8	16
9a	16	32	64	32	64	8	16
9b	8	16	32	16	32	8	16
9c	4	8	16	8	16	8	16
9d	16	32	64	32	64	8	16
9e	8	16	32	16	32	8	16
9f	16	32	64	32	64	8	16

3. EXPERIMENTAL SECTION

3.1 General

All reagents and solvents were obtained from commercial suppliers (Sigma-Aldrich, Alfa Aesar) and used without further purification unless otherwise stated. Melting points were measured on a Kofler apparatus and are reported uncorrected. IR spectra were recorded on a Shimadzu FTIR-8400S spectrophotometer (KBr pellets). ^1H and ^{13}C NMR spectra were acquired on a Bruker Avance 400 MHz instrument in DMSO-d_6 with TMS as internal standard. Mass spectra were obtained on a Shimadzu GCMS-QP2010 spectrometer using ESI ionisation. Elemental

analyses (C, H, N, S) were performed on a PerkinElmer 2400 CHNS/O analyser; all values were within ±0.4% of theoretical.

3.2 General Procedure for Synthesis of Bicyclic Intermediates

5-Substituted-2-hydroxybenzaldehyde (5-NO_2 or 5-Cl; 1.0 mmol), malononitrile (2.0 mmol), and 6-aminothiouracil (1.0 mmol) were combined in absolute ethanol (20 mL) with catalytic piperidine (0.1 mL) and heated under reflux for 6–8 h. Reaction progress was monitored by TLC (ethyl acetate/hexane, 3:7 v/v). After cooling to room temperature, the precipitate was collected by filtration, washed with cold ethanol (3 × 5 mL), and dried under vacuum to yield the bicyclic intermediates as pale yellow to orange solids.

3.3 General Procedure for Synthesis of Target Compounds 6a–6f and 9a–9f

To a stirred solution of the appropriate bicyclic intermediate (1.0 mmol) in anhydrous DMF (10 mL) were added the corresponding hydrazonyl halide (1.0 mmol) bearing the desired R substituent and Ar group, together with triethylamine (0.15 mL, 1.1 mmol). The mixture was stirred under N_2 at room temperature for 4–6 h, and completion was confirmed by TLC (chloroform/methanol, 9:1 v/v). The mixture was poured into ice-water (50 mL) with stirring; the precipitate was collected, washed with water (3 × 10 mL), and recrystallised from ethanol/DMF (4:1 v/v) to furnish the pure target compounds in 68–81% yield.

3.4 Computational Methods

Molecular docking was performed using Schrödinger Glide (XP mode) [23, 26]. Receptor structures were prepared with the Protein Preparation Wizard; grid boxes (20 × 20 × 20 Å) were centred on co-crystallised ligands. Three-dimensional ligand structures were built in Maestro, energy-minimised with the OPLS4 force field [22], and docked with full bond-rotation flexibility. MD simulations (100 ns) were conducted using Desmond (TIP3P solvent, NPT at 300 K / 1 atm, PME electrostatics, 10-Å cutoff). DFT calculations (B3LYP/6-311G(d,p)) [27, 28] were performed in Gaussian 09. In silico ADMET properties were predicted with pkCSM [24] and SwissADME; drug-likeness was evaluated by Lipinski's Rule of Five [25].

3.5 In Vitro Cytotoxicity Assay

Cytotoxicity against HCT-116 and MCF-7 cells was assessed by the MTT assay following the method of Mosmann [30]. Cells were maintained in DMEM (10% FBS, 2 mM L-glutamine, 1% penicillin/streptomycin) at 37 °C in 5% CO_2. After 24 h treatment with serial dilutions (0.1–100 µM), MTT was added, formazan crystals were dissolved in DMSO, and absorbance was read at 570 nm. IC_{50} values were calculated from dose–response curves by non-linear regression.

3.6 Antimicrobial Assay

Antimicrobial activities were determined by broth microdilution (CLSI guidelines) against S. aureus MRSA (ATCC 43300), E. coli (ATCC 25922), P. aeruginosa (ATCC 27853), C. albicans (ATCC 10231), and A. fumigatus (ATCC 16424). Ampicillin and fluconazole were used as reference controls. MIC is defined as the lowest concentration yielding no visible growth after 18–24 h incubation.

4. CONCLUSION

Design, synthesis, and characterization has been completed on twelve new hybrid heterocyclic compounds. Specifically, they are the series 6a-6f, 5-nitro, and 9a-9f, 5-chloro. These compounds were created through the condensation reaction between 5-substituted-2-hydroxybenzaldehydes with 6-aminothiouracil and a series of structurally different hydrazonyl halides with different R substituents, which included CH_3, OC_2H_5, furanyl, thiophenyl, NHC_6H_4, and aryl groups. A multi-level in silico and in vitro analysis was done, and the following main trends in the dataset were observed:

- With a molecular weight of 528.10 g/mol, Compound 9c (X = 5-Cl, R = furanyl, Ar = 4-$NO_2C_6H_4$) had the most favorable predicted binding affinity in the series, with ΔG_EGFR = −9.38 kcal/mol and ΔG_CDK2 = −8.72 kcal/mol, indicating potential as an EGFR/CDK2 inhibitor and warranting further studies.
- MD simulations predicted a stable binding mode for the EGFR–9c complex for 100 ns, with an average RMSD of 1.96 Å and a computed value of MM-GBSA = −68.7 ± 2.8 kJ/mol. Of the two, EGFR appeared to be the primary target, as opposed to CDK2, within the borders of the current computational environment.
- Moderate HOMO–LUMO gaps (3.39–3.61 eV) were found in all compounds from DFT analysis, and strong indices of electrophilicity (ω = 3.22–4.12 eV) were also found which may indicate favorable electronic interactions between the drugs and the target.
- The Lipinski assessment using corrected molecular weight (MW) values from the standalone compound table, suggests that only 4 out of 12 compounds (6a, 6d, 9a, 9d) are fully compliant with the Rule-of-Fives; the other 8 compounds have a MW greater than 500 g/mol,

which is a considerable limitation in drug-likeness of the present series.

- In the in vitro MTT assay, Compound 9c had the lowest IC_{50} value against HCT116 cells being 5.4 μM, which is approximately 2.2 times lower than 5-FU (12.1 μM) under the same conditions.
- The antimicrobial screening of 9c also exhibited the most potency in this dataset against MRSA S. aureus and C. albicans (MIC = 4 μg/mL), and this is on par with the reference standards.

With respect to the 6/9 series, the SAR analysis suggests two synergistic architectural principles: (a) 5-chloro substitution on the phenolic ring seems to confer greater potency in terms of antiproliferative and antimicrobial activity compared to 5-nitro, possibly due to better membrane permeability; and (b) a combination of a furanyl R substituent and a 4-nitrophenyl Ar group appears to exhibit the greatest activity in the present dataset, possibly due to synergistic hydrogen-bonding and electrostatic interactions at the active site of the EGFR.

Limitations and future directions: The most significant limitations are acknowledged. Most compounds in the series are above 500 g/mol according to the Lipinski rule; therefore, in future synthetic design, molecular weight reduction should be prioritized, in particular, substitutions of the R extending groups and simplification of the Ar group, while keeping the furanyl/4-nitrophenyl combination, which seems to be the driving force of the activity. The second point is that the in silico results presented here have not been in the laboratory confirmed with experimental binding assays (surface plasmon resonance, isothermal titration calorimetry, X-ray crystallography, etc.), and should be considered hypotheses. Third, to consider any of these compounds a clinical candidate, selectivity profiling against normal cell lines and in vivo pharmacokinetic/efficacy studies are mandatory. These studies are an active focus of our laboratory.

ACKNOWLEDGEMENTS

The authors gratefully acknowledge Faculty of Science, Benghazi, University of Benghazi for providing computational resources and laboratory infrastructure. No competing financial interests are declared.

REFERENCES

1. Anand U., Dey A., Chandel A.K.S., et al. Cancer chemotherapy and beyond: current status, drug candidates, associated risks and progress in targeted therapeutics. Genes Dis. 2022, 10, 1367–1401.
2. Aggarwal S. Targeted cancer therapies. Nat. Rev. Drug Discov. 2010, 9, 427–428.
3. Shosha M.I., El-Ablack F.Z., Saad E.A. New thiazole derivative as a potential anticancer and topoisomerase II inhibitor. Sci. Rep. 2025, 15, 710.
4. Indelicato S., Bongiorno D., Mauro M., Cascioferro S. Recent developments of 1,3,4-thiadiazole compounds as anticancer agents. Pharmaceuticals 2025, 18, 580.
5. Nikolova-Mladenova B., Momekov G., Ivanov D., Bakalova A. Salicylaldehyde benzoylhydrazones with anticancer activity and selectivity. J. Appl. Biomed. 2017, 15, 233–240.
6. Nikolova-Mladenova B., Halachev N., Iankova R., Momekov G., Ivanov D. Synthesis, characterization and cytotoxic activity of new salicylaldehyde benzoylhydrazone derivatives. Arzneimittelforschung 2011, 61, 714–718.
7. Yu H., Zhang W., Yu Q., et al. Ni(II) complexes with Schiff base ligands: preparation, characterization, DNA/protein interaction and cytotoxicity studies. Molecules 2017, 22, 1772.
8. Bulbul M.Z.H., Chowdhury T.S., Misbah M.M.H., et al. Synthesis of new series of pyrimidine nucleoside derivatives bearing acyl moieties as potential antimicrobial agents. Pharmacia 2021, 68, 23–34.
9. Maowa J., Hosen M.A., Alam A., Rana K.M., Fujii Y., Ozeki Y., Kawsar S.M.A. Pharmacokinetics and molecular docking studies of uridine derivatives as SARS-CoV-2 Mpro inhibitors. Phys. Chem. Res. 2021, 9, 385–412.
10. Kawsar S.M.A., Hosen M.A., Alam A., Islam M., et al. Thymidine derivatives as inhibitors against novel coronavirus (SARS-CoV-2) main protease: theoretical and computational investigations. Adv. Chem. Res. 2021, 69, 89–129.
11. Bulbul M.Z.H., Hosen M.A., Ferdous J., Misbah M.M.H., Kawsar S.M.A. Thermochemical, DFT study, physicochemical, molecular docking and ADMET predictions of modified uridine derivatives. Int. J. New Chem. 2021, 8, 88–110.
12. Alam A., Hosen M.A., Hosen A., Fujii Y., Ozeki Y., Kawsar S.M.A. Synthesis, characterization, and molecular docking against FimH receptor of E. coli (4XO8) of thymidine derivatives. J. Mex. Chem. Soc. 2021, 65, 256–276.

13. Hosen M.A., Alam A., Islam M., Fujii Y., Ozeki Y., Kawsar S.M.A. Geometrical optimization, PASS prediction, molecular docking, and in silico ADMET studies of thymidine derivatives against FimH adhesin of E. coli. Bulg. Chem. Commun. 2021, 53, 327–342.

14. Alam A., Rana K.M., Hosen M.A., et al. Modified thymidine derivatives as potential inhibitors of SARS-CoV: PASS, in vitro antimicrobial, physicochemical and molecular docking studies. Phys. Chem. Res. 2022, 10, 391–409.

15. Kawsar S.M.A., Hosen M.A. Thermochemical, DFT, molecular docking and pharmacokinetic studies of methyl β-D-galactopyranoside esters. J. Comput. Chem. Mol. Model. 2020, 4, 452–462.

16. Maowa J., Alam A., Rana K.M., et al. Synthesis, characterization, synergistic antimicrobial properties and molecular docking of sugar-modified uridine derivatives. Ovidius Univ. Ann. Chem. 2021, 32, 6–21.

17. Kawsar S.M.A., Kumar A. Computational investigation of methyl α-D-glucopyranoside derivatives as inhibitors against bacteria, fungi and COVID-19 (SARS-2). J. Chil. Chem. Soc. 2021, 66, 5206–5214.

18. Farhana Y., Amin M.R., Hosen M.A., et al. Monosaccharide derivatives: synthesis, antimicrobial, PASS, antiviral, and molecular docking studies against SARS-CoV-2 Mpro inhibitors. J. Cellul. Chem. Technol. 2021, 55, 477–499.

19. Esharkawy E.R., Almalki F.A., Ben Hadda T. In vitro potential antiviral activity of thymoquinone and dithymoquinone from Nigella sativa against SARS-CoV-19. Bioorg. Chem. 2022, 120, 105587.

20. Berredjem M., Bouzina A., Bahadi R., et al. Antitumor activity, X-ray crystallography, in silico study of N-sulfamido-phosphonates. J. Mol. Struct. 2022, 1250, 131886.

21. Burley S.K., Bhikadiya C., Bi C., et al. RCSB Protein Data Bank: powerful new tools for exploring 3D structures. Nucleic Acids Res. 2021, 49, D437–D451.

22. Harder E., Lu C., Wu C., et al. OPLS4: improving force field accuracy on challenging regimes of chemical space. J. Chem. Theory Comput. 2021, 17, 4291–4300.

23. Friesner R.A., Murphy R.B., Repasky M.P., et al. Extra precision Glide: docking and scoring incorporating a model of hydrophobic enclosure. J. Med. Chem. 2006, 49, 6177–6196.

24. Pires D.E.V., Blundell T.L., Ascher D.B. pkCSM: predicting small-molecule pharmacokinetic and toxicity properties using graph-based signatures. J. Med. Chem. 2015, 58, 4066–4072.

25. Lipinski C.A., Lombardo F., Dominy B.W., Feeney P.J. Experimental and computational approaches to estimate solubility and permeability in drug discovery and development. Adv. Drug Deliv. Rev. 2001, 46, 3–25.

26. Schrödinger LLC. Schrödinger Suite Release 2025-3. New York, NY, USA, 2025.

27. Becke A.D. Density-functional exchange-energy approximation with correct asymptotic behavior. Phys. Rev. A 1988, 38, 3098–3100.

28. Lee C., Yang W., Parr R.G. Development of the Colle-Salvetti correlation-energy formula into a functional of the electron density. Phys. Rev. B 1988, 37, 785–789.

29. Monks A., Scudiero D., Skehan P., et al. Feasibility of a high-flux anticancer drug screen using a diverse panel of cultured human tumor cell lines. J. Natl. Cancer Inst. 1991, 83, 757–766.

30. Mosmann T. Rapid colorimetric assay for cellular growth and survival: application to proliferation and cytotoxicity assays. J. Immunol. Methods 1983, 65, 55–63.